Supporting Information

Divalent Anion Salt Effects in Polyelectrolyte Multilayer Depositions

Walter J. Dressick[1a,*], Kathryn J. Wahl[1b], Nabil D. Bassim[1c],

Rhonda M. Stroud[1c], and Dmitri Y. Petrovykh[2,†,*]

[1] US Naval Research Laboratory
Divisions of Bio/Molecular Science & Engineering (Code 6910)[a], Chemistry (Code 6176)[b], and Materials Science (Code 6366)[c]
4555 Overlook Avenue, SW
Washington, DC 20375

[2] Department of Physics
University of Maryland
College Park, MD 20742

[†]Present address:
International Iberian Nanotechnology Laboratory (INL)
Avenida Mestre José Veiga
4715-330 Braga
Portugal

*Corresponding authors: walter.dressick@nrl.navy.mil and dmitri.petrovykh@inl.int

This file contains supporting information in the form of Materials and Methods, Tables, and Figures.

Materials and Methods

Materials. Deionized water (18 MΩ·cm) for all experiments was obtained from an Elix® 5 Milli-Q Plus Ultra-Pure Water System (Millipore Corp.). All organic solvents were ACS reagent Grade or better used as received from Sigma-Aldrich. Nitrogen gas was obtained from liquid N_2 boil-off via plumbed in-house lines and passed through a cellulose filter prior to use.

The following materials were used as received from the indicated commercial source, unless noted otherwise. Polyallylamine hydrochloride (PAH, M_w = 70,000 g·mole^{-1}, No. 28322-3), sodium polystyrenesulfonate (PSS, M_w = 70,000 g·mole^{-1}, No. 24305-1), sodium chloride (NaCl, 99.5%, No. S7653), sodium dihydrogen phosphate (NaH_2PO_4, > 99.0%, No. S8282), sodium fluoride (NaF, 99+%, No. 20,115-4), glacial acetic acid (HOAc, 99.99+%, No. 338826), sodium acetate ($NaC_2H_3O_2$, > 99.0%, No. S8750), disodium hydrogen phosphate (Na_2HPO_4, > 98%, anhydrous, No. S-7907), sodium oxalate ($Na_2C_2O_4$, ≥ 99.99%, No. 379735), disodium fumarate ($Na_2C_4H_2N_2O_4$, > 99%, No. F1506), sodium sulfate (Na_2SO_4, 99%, No. 23,391-3), magnesium chloride ($MgCl_2·6H_2O$, > 99.0%, No. M0250), ruthenium trichloride hydrate ($RuCl_3·H_2O$, > 98%, No. 206229), disodium bathophenanthrolinesulfonate (BPS, 98%, $Na_2C_{24}H_{14}N_2S_2O_6·3H_2O$, No. 14661-7), and 2, 2'-bipyridine (bpy, $C_{10}H_8N_2$, 99+%, No. D21630-5) were all from Sigma-Aldrich Chemicals. Magnesium sulfate ($MgSO_4$, ≥ 98.0%, No. BDH0246) was from BCH Chemicals Inc. and L-(+)-sodium tartrate ($Na_2C_4H_4O_6·2H_2O$, > 99.0%, No. BP352) was from Fisher Scientific. Disodium malonate ($Na_2C_3H_2O_4$, 99%, No. M0031), disodium succinate ($Na_2C_4H_4O_4·6H_2O$, > 98.0%, S0105), and disodium maleate ($Na_2C_4H_2N_2O_4$, > 99.0%, No. M0014) were from TCI America Inc. *N*-(2-aminoethyl)-3-aminopropyltrimethoxysilane (EDA, > 95%, No. SIA0591.0) from Gelest Inc. was purified by vacuum distillation (140-142°C; 14-15 mm Hg) immediately prior to use.

Ru Complexes. $Ru(bpy)_3(ClO_4)_2$ was initially prepared as the chloride salt by refluxing stoichiometric amounts of $RuCl_3$ and bpy ligand in 1:1 v/v ethanol: water under N_2 atmosphere for ca. 4 h. The crude product was isolated by evaporation of the solvent, dissolved in a minimum amount of water, and purified by ion exchange chromatography using a literature method [Ref 63, main text], followed by metathesis to the ClO_4^- salt prior to use. $Na_4Ru(BPS)_3$ was prepared from $RuCl_3$ and BPS by the literature method [Ref 61, main text].

Substrates. Polished quartz slides (No. 20200, 25.4 mm × 50.8 mm × 1 mm) were from Quartz Scientific Inc. Silicon wafers (100 mm diameter, 500–550 μm thickness, [100] orientation, p-type (B doping), resistivity 6–9 Ω, No. PD7403) from Wacker Siltronic Corp. were cut into 25×50 mm^2 pieces for use in the experiments.

Polyelectrolyte solutions. The presence of SO_4^{2-} and related dianions in solution during deposition of multilayers containing PAH greatly limits the available process window for film fabrication. For example, the dianion concentration must be kept below its gelation threshold value to provide stable polyelectrolyte solutions required for reproducible film deposition. In particular, for preparation of the μ=1.00 M PAH solutions with the various salts used in this work, we have found that gel formation is inhibited by addition of a concentrated salt solution containing NaCl and a salt of the dianion to be studied to a well-stirred solution of PAH in water. Concentrations of components are chosen with regard to solubility considerations and gelation threshold, as described in this work and the available literature. Our procedure produces stable solutions having appropriate levels of the dianion, NaCl, and PAH for PEML fabrication (Table S-1). In contrast, addition of the PAH solution to the concentrated salt solution leads to immediate or eventual (within ca. 1–2 days) gelation for several dianions studied.

The following example describes a typical preparation of a polyelectrolyte solution for fabrication of PEMLs in our work. To prepare the PAH deposition solution containing 2 mg PAH/mL 0.05 M Na_2SO_4/0.85 M NaCl, 350 mL of a solution containing 0.071 M Na_2SO_4 and 1.210 M NaCl was slowly added with stirring to an aqueous solution prepared by dissolving 1.00 g PAH in 150 mL water. Although some white cloudiness was observed during the initial stages of the addition, the solution became clear as the addition progressed. The solution was stirred for an additional 30 min and stored sealed in a Pyrex bottle for 2 days prior to use. Other solutions listed in Table S-1 were prepared in a similar manner.

Finally, because PAH contains primary alkylamine groups, solution pH must also be controlled to ensure that the degree of amine protonation remains approximately constant during our PEML deposition process regardless of which salt is present in solution. Kobayashi and coworkers [Ref 60, main text] have measured a $pK_a^{\mu = 1} \cong 9.67$ for PAH in μ = 1.00 M KCl (aq) solution and confirmed that it acts as a monobasic species. This value is ~0.9–1.0 pK unit lower than that expected for an aliphatic primary amine in aqueous solution ($\mu \rightarrow 0$), consistent with independent measurements of the general effect of μ on pK_a values in our solutions. Therefore, to maintain complete (*i.e.*, > 99%) protonation of the alkylamine sites of PAH in solution during PEML deposition, the PSS and PAH solutions must have pH ≤ 7.67. This requirement is met for all experiments (note Table S-1), ensuring consistent protonation of the PAH during multilayer fabrication regardless of the nature of the salt present.

PEML Deposition in Presence of Phosphate. We use HPO_4^{2-} dianion to provide a comparison with our results for SO_4^{2-} because both these anions possess two angled anionic sites ($P–O^-$ and $S–O^-$, respectively, see Chart 1, main text) capable of interacting with PAH amine sites at the solution pH used during film deposition (note Table S-1). The solution concentration of HPO_4^{2-}

used in our experiments is limited to a maximum level of ca. 0.011 M, with higher concentrations rapidly inducing gel formation. Nevertheless, PEMLs fabricated from solutions containing ca. 0.011 M HPO_4^{2-} dianion exhibit the largest absorbance and thickness values among the anions in Table 2, main text.

To develop a better understanding of the PEML deposition in presence of phosphate, we examined its ionization under our experimental conditions. For the reaction:

$$H_2PO_4^- \leftrightarrow H^+ + HPO_4^{2-} \quad \text{(S-1a)}$$

$$pK_a = pH + \log [HPO_4^{2-}]/[H_2PO_4^-] \quad \text{(S-1b)}$$

If $[HPO_4^{2-}] = [H_2PO_4^-]$, the logarithm term vanishes and $pK_a = pH$. Therefore, we prepared a μ = 1.00 M ionic strength solution containing 0.958 M NaCl, 0.011 M NaH_2PO_4, and 0.011 M Na_2HPO_4 and measured its $pH = pK_a = 6.29 \pm 0.03$. This value is ca. 0.9 pK units lower than the $pK_a = 7.21 \pm 0.01$ measured in water for the same reaction (*CRC Handbook of Chemistry and Physics, 79th Ed.*; Lide, D.R., Ed.; CRC Press: New York, 1999; p. **8**-45).

Given the solution pH of our experiments (*cf.*, Tables S-1 and S-5), the third P–OH site of HPO_4^{2-} will exist in the non-ionized P–OH form in solution in the absence of PAH. We speculate, however, that the superior performance of HPO_4^{2-} in PEML deposition experiments is a consequence of the potential deprotonation of that third P–OH site. Electrostatic binding of the two $P–O^-$ sites to protonated amines on the polyelectrolyte chain in PAH solution will alter the local environment of the remaining P–OH site. Spontaneous deprotonation of the remaining P–OH site would permit formation of an additional electrostatic interaction with an adjacent PAH protonated amine, further stabilizing the $(PAH–NH_3^+)_2\cdots HPO_4^{2-}$ interface as shown in eq. (S-2):

$$(P–NH_3^+)_2\cdots HPO_4^{2-} + P–NH_3^+ \rightarrow H^+ + (P–NH_3^+)_3\cdots PO_4^{3-} \quad \text{(where } P–NH_3^+ \text{ is PAH)} \quad \text{(S-2)}$$

Although our data are insufficient to confirm this hypothesis and a detailed analysis requiring additional experiments is beyond the scope of this work, the extreme pH sensitivity of the HPO_4^{2-} bridging phenomenon, which is quenched via addition of a proton to form $H_2PO_4^-$, is certainly consistent with such a mechanism.

Quantification of Ru-stained PEMLs. The release of $Ru(BPS)_3^{4-}$ dye from the PAH during PSS treatment described in Section 2.3 of the main text indicates that separate populations of strongly and weakly bound dye exist in the terminal PAH layer of the growing PSS/PAH/Ru film. Therefore, at least two separate environments, presumably corresponding to extended and coiled PAH chains [Ref 28, main text], are present in the terminal PAH layer during dye deposition. Figure 3C indicates that the process described above leads to reproducible fabrication of PEMLs comprising PSS/PAH/Ru trilayers. Linear plots of absorbance *vs*. number of PSS/PAH/Ru trilayers are observed at 225 nm, 286 nm, and 460 nm. The linearity of the plot at 225 nm, where both the PSS and Ru complex absorb light, is consistent with maintenance of the reproducible linear film growth mode exhibited by the corresponding PSS/PAH bilayer PEML shown in Figure 3A. The ratio of the slopes for the 286 nm and 460 nm plots (*i.e.*, $(0.093 \pm 0.002)/(0.024 \pm 0.001) \cong 3.87 \pm 0.23$), where only the Ru dye absorbs light, is equivalent to the extinction coefficient ratio for the solution phase Ru complex (*i.e.*, $\varepsilon'(286\text{ nm})/\varepsilon'(460\text{ nm}) = (9.08 \pm 0.09) \times 10^4\ \text{L}\cdot\text{mole}^{-1}\cdot\text{cm}^{-1}/(2.50 \pm 0.03) \times 10^4\ \text{L}\cdot\text{mole}^{-1}\cdot\text{cm}^{-1} \cong 3.63 \pm 0.08$). This behavior, together with the agreement between the solution and film spectra of the Ru dye in Figure 3B, indicates that incorporation of the Ru complex into the PEML occurs without degradation (note also Figure S-3). Although the PSS/PAH/Ru trilayer PEMLs contain less PSS than the corresponding PSS/PAH bilayer films prepared from 0.04 M Na_2SO_4/0.88 M NaCl (aq) polyelectrolyte solutions, film thickness is increased. In fact, a Si-EDA/$(PSS/PAH/Ru)_{20}$ film exhibits a

PSS/PAH/Ru trilayer thickness of ~9.0 ± 0.2 nm compared to a PSS/PAH bilayer thickness of ~7.6 ± 0.1 nm for the corresponding Si-EDA/$(PSS/PAH)_{20}$ film in Table 3, main text. However, the change in thickness is accompanied by little increase in roughness, with r_q values of 1.34 ± 0.14 nm and 1.22 ± 0.09 nm determined for the Si-EDA/$(PSS/PAH/Ru)_{20}$ and Si-EDA/$(PSS/PAH)_{20}$ films, respectively.

Quantification of Amine and Sulfonate Sites. The $Ru(bpy)_3(ClO_4)_2$ and $Na_4Ru(BPS)_3$ complexes (Chart 1, main text) were also used to estimate the relative concentrations of available amine and sulfonate sites present on terminal PSS and PAH polyelectrolyte layers, respectively, for PSS/PAH multilayers deposited from 0.037 M Na_2SO_4/0.889 M NaCl solutions. A Q-EDA/$(PSS/PAH)_2$/PSS film was treated 4 h with aqueous 4.3×10^{-4} M $Ru(bpy)_3(ClO_4)_2$ solution, followed by a triple water rinse, to electrostatically bind $Ru(bpy)_3^{2+}$ cation to available $-SO_3^-$ groups present in the terminal PSS layer of the film. Analogous treatment of a Q-EDA/$(PSS/PAH)_2$ film with aqueous 4.0×10^{-4} M $Na_4Ru(BPS)_3$ solution bound $Ru(BPS)_3^{4-}$ anion to available $-NH_3^+$ sites on the terminal PAH layer in this film. Binding occurs without decomposition of the dyes, as shown by maintenance of dye fluorescence in the films (note Figure S-3) and observation of their characteristic metal-to-ligand charge-transfer (MLCT) absorbance bands near ~460 nm. The surface concentration of each adsorbed Ru complex (*i.e.*, [Ru], mole·cm^{-2}) was estimated from the UV-visible absorbance of the multilayer film (*i.e.*, $A/2$, where the factor "2" accounts for the presence of multilayer film on both sides of the quartz substrate) and its extinction coefficient (*i.e.*, ε, cm^2·mole^{-1}) via Beer's law using eq. (S-3):

$$[Ru] = A/(2\varepsilon) \qquad \text{(S-3)}$$

Taking a ratio of [Ru] terms from eq. (S-3) for the bound $Ru(BPS)_3^{4-}$ and $Ru(bpy)_3^{2+}$ species and recognizing that each $Ru(bpy)_3^{2+}$ cation could bind at most two $-SO_3^-$ groups and each

$Ru(BPS)_3^{4-}$ anion could bind at most six $-NH_3^+$ groups leads, after some simplification, to eq. (S-4) as an estimate of the ratio of available amine sites at a terminal PAH layer to available sulfonate sites on a terminal PSS layer, $[-NH_3^+]/[-SO_3^-]$:

$$[-NH_3^+]/[-SO_3^-] \cong A'\varepsilon''/(3A''\varepsilon') \quad \text{(S-4)}$$

In eq. (S-4), A' and ε' are values associated with bound $Ru(BPS)_3^{4-}$ anion and A'' and ε'' are values associated with bound $Ru(bpy)_3^{2+}$ cation. The $\varepsilon' = 2.5\times10^7$ $cm^2\cdot mole^{-1}$) and $\varepsilon'' = 1.4\times10^7$ $cm^2\cdot mole^{-1}$ values for the metal-to-ligand charge-transfer (*i.e.*, MLCT) absorbance band at ~460 nm appropriate for complexes adsorbed to the polyelectrolyte surfaces were calculated from corresponding ε ($L\cdot mole^{-1}\cdot cm^{-1}$) values measured from UV-visible absorption maxima for aqueous solutions containing known concentrations of each complex using eq. (S-5):

$$\varepsilon\ (cm^2\cdot mole^{-1}) = \varepsilon\ (L\cdot mole^{-1}\cdot cm^{-1}) \times 1000\ cm^3\cdot L^{-1} \quad \text{(S-5)}$$

Use of eq. (S-4) is strictly valid only if binding of the complex to the polyelectrolyte layer does not affect the oscillator strength of the electronic transition corresponding to the absorbance band. In fact, small shifts in the positions and bandwidths of the absorbance peak maxima are observed for both complexes in our experiment after binding to the polyelectrolyte layer (*vide infra*), suggesting that some small change in ε likely occurs. Therefore, we select absorbance bands of the same parentage in each complex (*i.e.*, MLCT $d\pi-\pi^*$) for the calculation in eq. (S-4) in order to minimize the effect of ε perturbations.

Light Scattering. A NanoSight LM10-HSBF nanoparticle size determination system (www.nanosight.com; Nanosight Worthington, OH, USA) equipped with He-Ne laser for light scattering measurements was used for polyelectrolyte aggregate detection and analysis in solution. The Brownian motion of polyelectrolyte aggregates in 0.04 M Na_2SO_4/0.88 M NaCl and 1.00 M NaCl solutions was tracked and analyzed using the software supplied with the instrument

to estimate the hydrodynamic radii and concentrations of any particles present. Because the Nanosight NTA2.1 software was designed to determine the size of hard shell spherical particles, the system cannot provide absolute values for particle size for our polyelectrolyte aggregates having fluxional surface boundaries and shapes. Nevertheless, relative comparisons of the derived parameters for the various polyelectrolytes and solution conditions examined can still be made to provide qualitative information concerning the nature of any aggregates present for samples examined under identical acquisition conditions.

Specifically, in our experiments, the instrument sample solution platen was first rinsed with a salt solution having the same composition as the polyelectrolyte solution to be analyzed and wiped dry with a KimWipe^{TM} lint-free paper towel. The polyelectrolyte solution containing 2 mg/mL of PAH or PSS in either 0.04 M Na_2SO_4/0.88 M NaCl or 1.00 M NaCl solution was then applied to the platen and particle Brownian motion was recorded at room temperature for 60 s to obtain a video for analysis. Relative brightness (*i.e.*, 0), gain (*i.e.*, 1.00), and blur size (*i.e.*, 5 pixel x 5 pixel) settings were the same for all samples and the detection threshold was automatically adjusted by the software. Each experiment was repeated 4–8 times to obtain average values and standard deviations for the particle mean diameter, D_{50} (*i.e.*, particle median) value, and particle concentration. After removal of the sample solution, the platen was rinsed twice with salt solution having the same composition as the polyelectrolyte solution just analyzed. It was then rinsed successively with water, 70:30 v/v ethanol:water, and water again before being dried with a lint-free paper towel to complete the cleaning process before measurement of the next sample. Control experiments were performed using polyelectrolyte-free 1.00 M NaCl and 0.04 M Na_2SO_4/0.88 M NaCl solutions. Because the results for these controls indicated that the polyelectrolyte-free salt solutions contained essentially no particles (*i.e.*, > 100-fold less than analo-

gous solutions containing the polyelectrolytes), no corrections were made to the data obtained for our polyelectrolyte solutions.

AFM Characterization. AFM experiments were performed on a Veeco Nanoman AFM in tapping mode (intermittent contact mode) using TESP tips with nominally 20 nm tip radii. AFM measurements were made in air to assess sample surface topography, surface roughness, and film thickness. At least 3 images per sample were acquired from regions away from film edges for evaluations of surface topography and roughness. Images for topography evaluation were typically acquired at 10 × 10 μm scan sizes, with occasional additional measurements made as necessary at 20 × 20 μm, 5 × 5 μm, and 2 × 2 μm scan sizes. Roughness measurements were made in a 25 μm^2 region (typically 5 × 5 μm) after processing the image using a flattening routine in the instrument software.

Samples were prepared for AFM measurement of total PEML film thickness by gently scribing PEMLs deposited onto the Si-EDA (or Q-EDA) substrate with stainless steel microscope tweezers to create a step edge boundary for the measurement. The scribing was not found to damage the substrate surface. To determine whether any PSS/PAH layers were left after scribing, representative samples were more aggressively scribed using tweezers or a razor blade. AFM measurements indicated removal of a small additional amount of material (~1 nm) consistent with loss of the EDA monolayer from these surfaces, which was observed as a brighter region by optical microscopy (the EDA appearing darker than the native silicon under a microscope objective). While this observation does not prove that there are no PEMLs remaining on the substrate, it is likely that the scribing provides a reasonable and consistent method to assess multilayer thickness.

In some cases we also measured the thickness increase noted following deposition of a PAH layer to a PSS-terminated PEML. Samples for this measurement were prepared by dipping only a portion of the substrate bearing the PSS-terminated PEML into the PAH treatment solution, thereby creating a PSS-PAH step edge boundary to facilitate the measurement. For both the incremental PAH thickness increase and total PEML film thickness, measurements were made by scanning the AFM tip across each step edge boundary at a right angle. A minimum of 18 such measurements were made for each thickness determination, with the average thickness reported. The error for the total film thickness is reported as the standard deviation of the data. The errors reported for the PSS/PAH bilayer thickness and the PAH layer thickness are calculated using the propagation of errors method (chain rule calculus).

Table S-1. Salt Solution Compositions and pH Values

Salt Identity[a]	**Solution Composition**[b]	**Solution pH**[c]		
		Rinse[d]	**PSS**[e]	**PAH**[f]
NaCl	1.00 M NaCl	6.50[g]	6.47	4.58
NaF	0.05 M NaF / 0.95 M NaCl	7.35[h]	7.46[h]	5.75
NaH_2PO_4	0.05 M NaH_2PO_4 / 0.95 M NaCl	4.18	4.20	4.03
Na(Acetate)	0.05 M $H_3CCOONa$ / 0.95 M NaCl	7.11	6.97	6.50
$MgCl_2$	0.05 M $MgCl_2$ / 0.85 M NaCl	6.77	6.46	5.14
$MgSO_4$	0.05 M $MgSO_4$ / 0.80 M NaCl	6.52	6.40	5.09
Na_2SO_4	0.05 M Na_2SO_4 / 0.85 M NaCl	6.97	6.91	6.05
Na_2HPO_4	0.011 M Na_2HPO_4 / 0.010 M NaH_2PO_4 / 0.967 M NaCl	6.25	6.25	6.15
Na_2Oxalate	0.05 M $Na_2C_2O_4$ / 0.85 M NaCl	7.57[h]	7.39[h]	6.40
Na_2Tartrate	0.05 M NaOOCCH(OH)CH(OH)COONa / 0.85 M NaCl	6.68	6.67	6.05
Na_2Maleate	0.05 M *cis*-NaOOCCH=CHCOONa / 0.85 M NaCl	8.12[h]	7.69[h]	7.19
Na_2Fumarate	0.05 M *trans*-NaOOCCH=CHCOONa / 0.85 M NaCl	7.00	6.72	6.07
Na_2Malonate	0.05 M $NaOOCCH_2COONa$ / 0.85 M NaCl	7.42	7.28	6.86
Na_2Succinate	0.05 M $NaOOC(CH_2)_2COONa$ / 0.85 M NaCl	7.17	7.28	6.85

[a] Identity of the unique salt present in each polyelectrolyte solution during the deposition of the multilayer films.

[b] Composition of the salt solution showing the concentrations of the unique salt tested and added NaCl to adjust total solution ionic strength μ = 1.00 M.

[c] pH of freshly prepared solution measured at 23 ± 2°C. Std. dev. = 0.03 pH units (from 3 measurements).

[d] pH of the first multilayer film rinse solution having the composition shown in column 2 and used in the salt rinse protocol (see Materials and Methods).

[e] pH of the solution shown in column 2 also containing 2 mg PSS polyelectrolyte / mL solution and used for multilayer deposition.

[f] pH of the solution shown in column 2 also containing 2 mg PAH polyelectrolyte / mL solution and used for multilayer deposition.

[g] 1.00 M NaCl (aq) solution having this pH is also used as the second rinse solution in the salt rinse protocol (see Materials and Methods).

[h] Solution pH dropped ~0.1-0.3 units after repeated solution exposure to the air during normal use due to slow adsorption of carbon dioxide.

Table S-2. Light Scattering Analysis of PAH and PSS Salt Solutions

Solution Composition[a]	No.[b]	Mean Diameter[c] (nm)	D_{50} Value[d] (nm)	Particle Concentration[e] (particles/mL)
PAH (0.04 M Na_2SO_4/0.88 M NaCl)	8	133 ± 27	116 ± 16	$(9.35 \pm 0.98) \times 10^8$
PSS (0.04 M Na_2SO_4/0.88 M NaCl)	7	147 ± 16	138 ± 12	$(3.53 \pm 1.13) \times 10^8$
PAH (1.00 M NaCl)	4	186 ± 10	183 ± 9	$(1.50 \pm 0.18) \times 10^8$
PSS (1.00 M NaCl)	4	144 ± 3	128 ± 17	$(6.02 \pm 2.45) \times 10^8$

[a] Identity of polyelectrolyte and salt in solution analyzed. Polyelectrolyte is present at 2 mg/mL in each solution. Fresh polyelectrolyte solution was used for each measurement. Sample platen was prepared as described in the Materials and Methods.

[b] Number of measurements made.

[c] Estimated average polyelectrolyte aggregate diameter ± standard deviation in nm.

[d] Estimated polyelectrolyte aggregate size ± standard deviation in nm for which half the aggregates are larger and half are smaller.

[e] Estimated polyelectrolyte aggregate concentration ± standard deviation in particles/mL solution.

Table S-3. Dependence of Multilayer Films Properties on Solution Sulfate Concentration Associated with Figure 2A (Salt Rinse Protocol)

Salt[a] **(Substrate)**[b]	**Concentration**[c]		**Abs.**[d]	**Thickness (nm)**		**Roughness (nm)**	
	Na_2SO_4	NaCl		**Total Film**[e]	**Bilayer**[f]	$\mathbf{r_q}$[g]	**N**[h]
NaCl (Q)	0.00	1.00	0.7558	–––	–––	–––	–
NaCl (Si)	0.00	1.00	–––	97.5 ± 2.2	4.10 ± 0.1	0.8 ± 0.4	3
Na_2SO_4 (Q)	0.05	0.85	1.8176	226.8 ± 3.7	11.3 ± 0.2	1.14 ± 0.1	3
Na_2SO_4 (Si)	0.05	0.85	–––	274.2 ± 12.8	11.4 ± 0.5	–––	–
Na_2SO_4 (Q)	0.043	0.871	1.2806	–––	–––	–––	–
Na_2SO_4 (Si)	0.043	0.871	–––	175.1 ± 0.2	7.3 ± 0.1	0.64 ± 0.03	3
Na_2SO_4 (Q)	0.04	0.88	1.2425	–––	–––	–––	–
Na_2SO_4 (Si)	0.04	0.88	–––	151.5 ± 1.9	7.6 ± 0.1	1.22 ± 0.09	3
Na_2SO_4 (Q)	0.037	0.889	1.1105	–––	–––	–––	–
Na_2SO_4 (Si)	0.037	0.889	–––	148.0 ± 2.3	6.2 ± 0.1	1.5 ± 1.0	5
Na_2SO_4 (Q)	0.03	0.91	0.9785	–––	–––	–––	–
Na_2SO_4 (Si)	0.03	0.91	–––	134.6 ± 3.0	5.6 ± 0.1	0.8 ± 0.3	3
Na_2SO_4 (Q)	0.01	0.97	0.8061	–––	–––	–––	–––
Na_2SO_4 (Si)	0.01	0.97	–––	103.5 ± 1.1	4.3 ± 0.1	0.9 ± 0.1	3

[a] Identity of the salt present in each polyelectrolyte solution (and initial rinse solution for sulfate-containing solutions) during multilayer deposition.

[b] Identity of the substrate coated with the multilayer. Q = quartz and Si = silicon wafer. Substrates were coated with a chemisorbed EDA organosiloxane monolayer prior to multilayer deposition. Multilayer films have structure: Substrate-EDA/$(PSS/PAH)_x$ (x =20 for quartz (Q) and x = 24 for silicon (Si) substrates).

[c] Left column indicates the molar concentration of Na_2SO_4 in the polyelectrolyte treatment solution and first rinse solutions. Right column indicates the concentration of NaCl present to bring the solution ionic strength to μ = 1.00 M.

[d] UV absorbance of the multilayer film at 225 nm on a quartz substrate.

[e] Thickness (± std. dev.) of the multilayer film as determined by AFM.

[f] Average thickness (± std. dev.) of a single PSS/PAH bilayer within the multilayer film, calculated by division of the total film thickness by the number of bilayers deposited, "x", with x = 20 (quartz) or x = 24 (Si).

[g] Root-mean-square roughness, r_q, (± std. dev.) from AFM measurements.

[h] Number of measurements taken to determine roughness values.

Table S-4. Absorbance Data for PAH/PSS/Ru(bathophenanthrolinesulfonate)$_3^{4-}$ Trilayer-based Multilayer Films Associated with Figures 3B and 3C

Row	Trilayer No.[a]	Film Structure[b]	Abs.[c] (225 nm)	Abs.[c] (286 nm)	Abs.[c] (464 nm)
1[d, e]	3	[(PSS/PAH/Ru[f])$_3$/PSS/PAH]	0.37026	0.303833	0.093956
2[e, g]	4	[(PSS/PAH/Ru)$_4$]	0.494527	0.461827	0.147875
3[g, h]	4	[(PSS/PAH/Ru)$_4$/PSS]	0.468506	0.392885	0.127366
4[d, h]	4	[(PSS/PAH/Ru)$_4$/PSS/PAH]	0.454794	0.385262	0.127633
5[d]	7	[(PSS/PAH/Ru)$_7$/PSS/PAH]	0.792142	0.597925	0.20253
6[d]	8	[(PSS/PAH/Ru)$_8$/PSS/PAH]	0.933085	0.704562	0.224804
7[d]	9	[(PSS/PAH/Ru)$_9$/PSS/PAH]	1.0654	0.818163	0.242362
8[h]	10	[(PSS/PAH/Ru)$_{10}$/PSS]	1.185596	0.917511	0.259185
9[d, e, h]	10	[(PSS/PAH/Ru)$_{10}$/PSS/PAH]	1.176532	0.917933	0.254785
10[e, g]	11	[(PSS/PAH/Ru)$_{11}$]	1.320172	1.101638	0.291548
11[g, h]	11	[(PSS/PAH/Ru)$_{11}$/PSS]	1.29084	1.028493	0.273427
12[d, h]	11	[(PSS/PAH/Ru)$_{11}$/PSS/PAH]	1.284034	1.021332	0.271213
13[d]	12	[(PSS/PAH/Ru)$_{12}$/PSS/PAH]	1.399545	1.117805	0.293125
14[d]	13	[(PSS/PAH/Ru)$_{13}$/PSS/PAH]	1.526528	1.22435	0.314943
15[d]	16	[(PSS/PAH/Ru)$_{16}$/PSS/PAH]	1.910164	1.481669	0.397298
16[d]	16	[(PSS/PAH/Ru)$_{16}$/PSS/PAH]	1.907305	1.478812	0.398347
17[d]	16	[(PSS/PAH/Ru)$_{16}$/PSS/PAH]	1.908482	1.479037	0.403783
18[d]	18	[(PSS/PAH/Ru)$_{18}$/PSS/PAH]	2.14154	1.679246	0.474377
19[d, e]	19	[(PSS/PAH/Ru)$_{19}$/PSS/PAH]	2.266959	1.79541	0.509651
20[e]	20	[(PSS/PAH/Ru)$_{20}$]	2.434432	1.978641	0.565566

[a] Number of PAH/PSS/Ru(bathophenanthrolinesulfonate)$_3^{4-}$ trilayers present in the film.

[b] Internal structure of the multilayer film on the EDA-coated quartz slide (not shown). Polyelectrolyte layers were deposited from separate solutions containing 2 mg PSS or PAH / mL of 0.04 M Na_2SO_4/0.85 M NaCl solution. Polyelectrolyte layers were sequentially rinsed using 0.04 M Na_2SO_4/0.85 M NaCl solution, 1.00 M NaCl solution, and water according to the salt rinse protocol. The Ru deposition solution comprised 2 mg Na_4Ru(bathophenanthrolinesulfonate)$_3$ / mL water. The Ru layers were triple rinsed in water. Films were dried in a filtered N_2 gas stream after deposition of each layer.

[c] UV-visible film absorbance of the indicated wavelength. Uncertainty is ±0.005 abs. units.

[d] Data for films in these rows are used to prepare the plot shown in Figure 3C.

[e] Comparison of data in adjacent rows marked "*e*" indicates the effect on absorbance of the addition of a Ru layer to a film terminated by a PAH layer, *e.g.*, rows 1 *vs*. 2, 9 *vs*. 10.

[f] "Ru" represents the Ru(bathophenanthrolinesulfonate)$_3^{4-}$ transition metal complex ion, where bathophenanthrolinesulfonate is 4, 7-di-(*m*-sulfonatophenyl)-1, 10-phenanthroline, in each film structure.

[g] Comparison of data in adjacent rows marked "*g*" indicates the effect on film absorbance of the addition of a PSS layer to the multilayer film terminated by a Ru layer, *e.g.*, rows 2 *vs*. 3.
[h] Comparison of data in adjacent rows marked "*h*" indicates the effect on film absorbance of the addition of a PAH layer to the multilayer film terminated by a PSS layer, *e.g.*, rows 3 *vs*. 4.

Table S-5. Correlation of Film Absorbance and Thickness with Ion Jones-Dole *B* Parameters

Ion Name (Formula)[a]	**ID**[b]	**pK_a**[c]	***B***[d]	**A(225 nm)**[e]	**Bilayer Thickness (Std. Dev.)**[f]
Chloride (Cl^-)	CL	–––	–0.005[g]	0.7558	4.1 (0.1)
Fluoride (F^-)	F	–––	0.107[g]	0.7620	3.9 (0.34)
Oxalate ($C_2O_4^{2-}$)	OX	4.19	0.164[h]	1.4746	9.4 (0.5)
Sulfate (SO_4^{2-})	S	–––	0.206[g]	1.8176	11.4 (0.5)
Acetate (CH_3COO^-)	AC	4.76	0.227[h]	0.7412	3.78 (0.07)
Malonate $CH_2(COO^-)_2$	MN	4.69	0.285[h]	0.8335	4.8 (0.1)
Dihydrogenphosphate ($H_2PO_4^-$)	DP	7.21	0.340[g]	0.7434	4.00 (0.04)
Maleate *cis*-$^-$OOCCH=CHCOO$^-$	ML	6.07	0.348[h]	0.9829	6.0 (0.1)
Fumarate *trans*-$^-$OOCCH=CHCOO$^-$	FT	4.44	0.377[h]	0.7970	4.3 (0.1)
Monohydrogenphosphate (HPO_4^{2-})[i]	MP	12.32	0.382[g]	1.9078	12.0 (0.2)
Succinate $^-$OOCCH$_2$CH$_2$COO$^-$	SC	5.61	0.418[h]	0.7826	4.0 (0.4)
Tartrate $^-$OOCCH(OH)CH(OH)COO$^-$	TR	4.34	0.469[h]	1.0557	5.67 (0.09)

[a] Ion concentrations are 0.05 M as Na^+ salts, except where noted, with sufficient added NaCl to give a μ = 1.00 M ionic strength in solution.

[b] Abbreviation used to identify ions in Figure S-5.

[c] pK_a (25°C, $\mu \rightarrow 0$) for the reaction $HB^- \leftrightarrow H^+ + B^{2-}$ (OX, MN, ML, FT, SC, and TR), for the reaction $HB \leftrightarrow H^+ + B^-$ (AC), for the reaction $H_2B^- \leftrightarrow H^+ + HB^{2-}$ (DP), and for the reaction $HB^{2-} \leftrightarrow H^+ + B^{3-}$ (MP). Values are taken from: *CRC Handbook of Chemistry and Physics, 79th Ed.*; Lide, D.R., Ed.; CRC Press: New York, **1999**; pp. **8**-43 – **8**-46. Estimates for corresponding pK_a values in our μ = 1.00 M solutions are obtained by subtraction of ~0.9 from each value as explained in Materials and Methods.

[d] Jones-Dole viscosity *B* coefficient in water at 25°C from the indicated reference.

[e] Absorbance at 225 nm for a quartz slide coated on both sides with a film of structure Q-EDA/(PSS/PAH)$_{20}$.

[f] Thickness (and standard deviation) in nm of a PSS/PAH bilayer calculated from AFM measurement of the total thickness of a film deposited on Si wafer having structure Q-EDA/(PSS/PAH)$_{24}$.

[g] *B* value taken from Ref 75, main text.

[h] *B* value taken from: Ref 76, main text.

[i] The HPO_4^{2-} ion is present at 0.011 M in a solution also containing 0.010 M $H_2PO_4^-$ and 0.967 M NaCl at pH ~6.25 (PSS and rinse solutions) or pH = 6.15 (PAH solution).

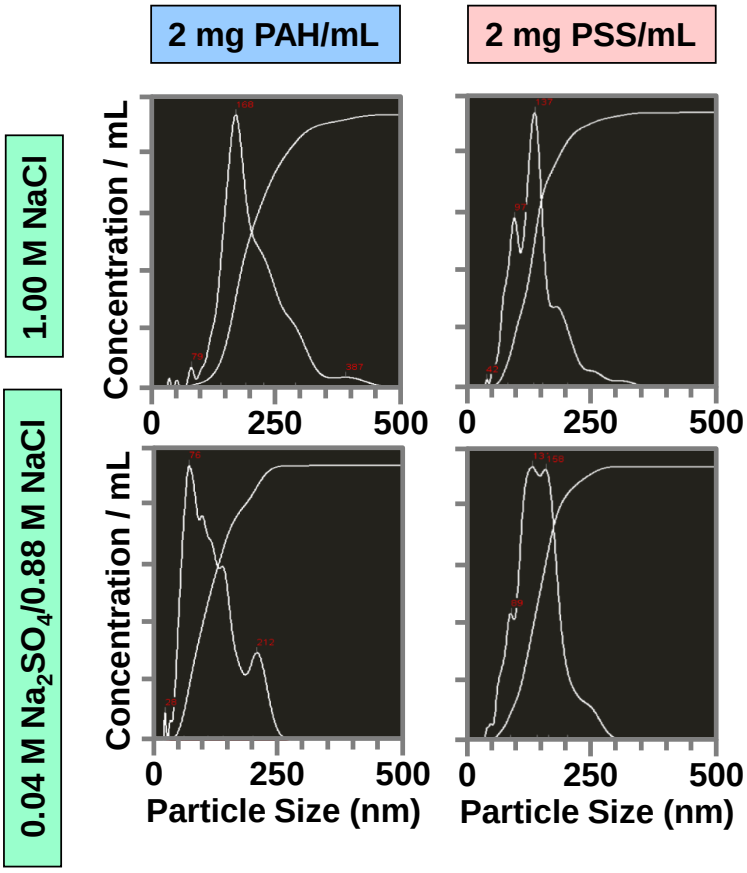

Figure S-1: Light scattering results presented as relative particle concentrations *vs*. particle size are shown for PSS and PAH polyelectrolytes in 1.00 M NaCl(aq) and 0.04 M Na_2SO_4/0.88 M NaCl (aq) solutions. The particle size distribution (left curve) and integrated distribution curve (right curve) for polyelectrolyte aggregates present in each solution are shown. Consult Table S-2 for additional information.

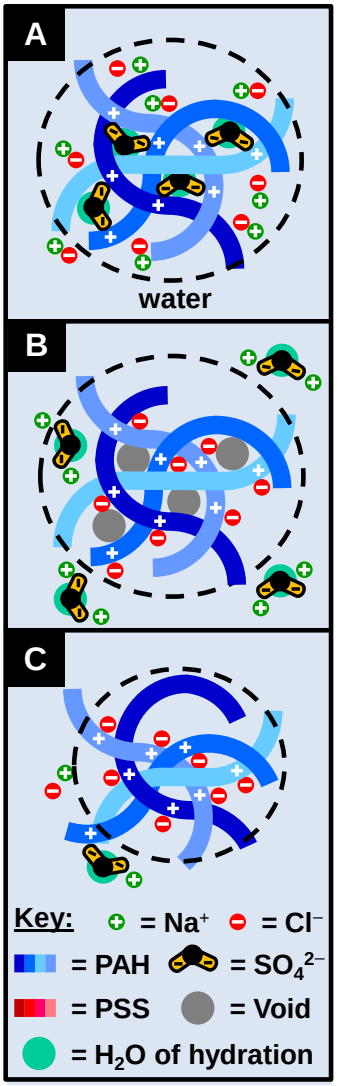

Figure S-2: Rinsing model for PAH particle precipitation. An intact PAH aggregate in a μ = 1.00 M ionic strength solution is diluted in water (Part A). Expulsion of excess SO_4^{2-} from the aggregate, accompanied by partial deprotonation of the PAH amine N sites and Cl^- exchange to maintain electroneutrality, occurs (Part B). Because SO_4^{2-} tightly binds and organizes water in its vicinity, its removal during dilution dehydrates the aggregate. Subsequent collapse of the PAH chains to fill the voids left by the rapidly departing SO_4^{2-} anions permits formation of stabilizing hydrogen bonds among deprotonated amine N sites on the PAH chains, raising the local PAH concentration above its solubility in water and precipitating the PAH particle (Part C). (The various shades of blue (PAH) polyelectrolyte strands serve solely to illustrate the chain entanglement described by the model.)

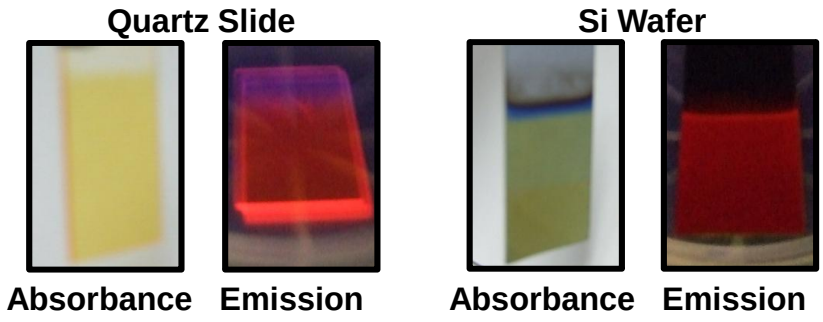

Figure S-3: A quartz slide (left) coated by a PEML of structure Q-EDA/(PSS/PAH/Ru)$_{20}$ (where Ru ≡ Ru(BPS)$_3^{4-}$) and a Si wafer (right) coated by a Si-EDA/(PSS/PAH/Ru)$_{19}$/PSS/PAH PEML are shown. The coated quartz slide exhibits the orange-yellow color associated with the Ru(BPS)$_3^{4-}$ chromophore. The PEML coated onto the Si wafer exhibits a green-yellow interference color reflecting contributions from the Ru(BPS)$_3^{4-}$ chromophore absorbance and the total PEML thickness. Both the coated quartz slide and Si wafer exhibit the characteristic red-orange emission during excitation at 254 nm associated with the Ru(BPS)$_3^{4-}$ MLCT excited state. Note the reflection of the quartz slide emission in the Fluoroware™ container. Additional information is presented in Table S-4 and Figures 3B and 3C.

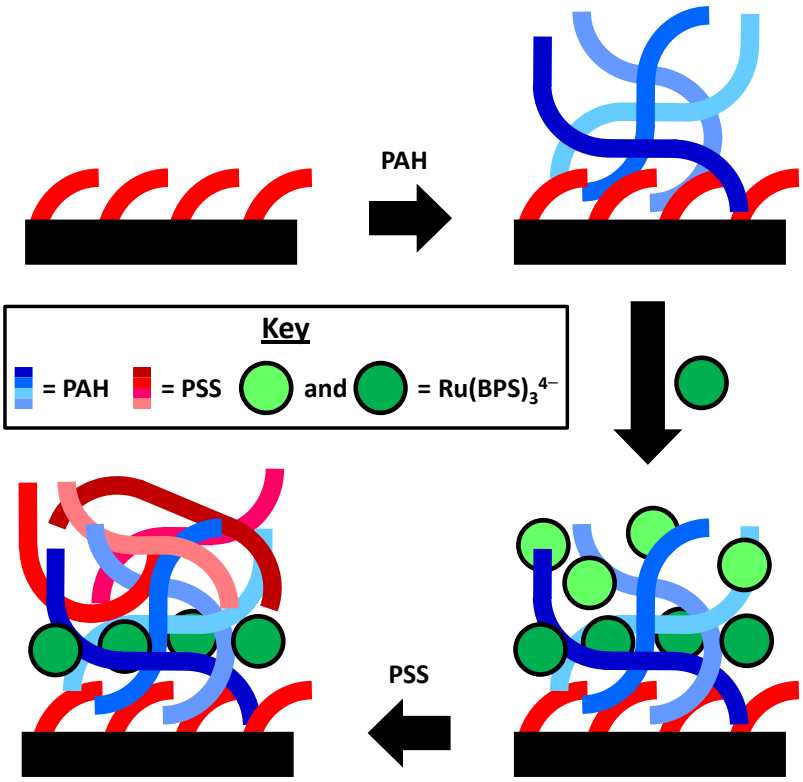

Figure S-4: Model for fabrication of PEMLs comprising PSS and $Ru(BPS)_3^{4-}$ dye-stained PAH. The model illustrates deposition of a single PSS/PAH/Ru trilayer. Weakly and strongly adsorbed $Ru(BPS)_3^{4-}$ dye species are indicated by light and dark green spheres, respectively. Additional information is contained in Figures 3B and 3C and Table S-4. (The various shades of blue (PAH) and red (PSS) polyelectrolyte strands serve solely to illustrate the chain entanglement described by the model.)

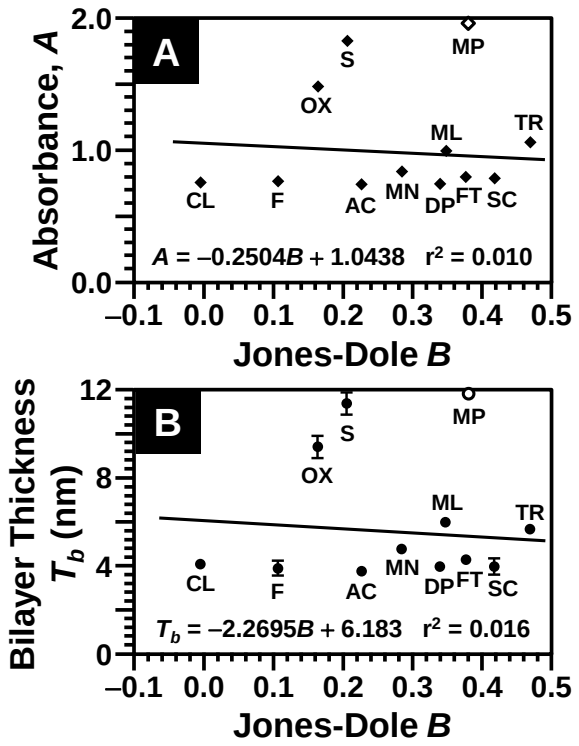

Figure S-5: Hofmeister correlations of salt anion Jones-Dole *B* viscosity parameter with (A) the absorbance at 225 nm, *A*, for each Q-EDA/$(PSS/PAH)_{20}$ PEML and (B) the PSS/PAH bilayer thickness, T_b, for each Si-EDA/$(PSS/PAH)_{24}$ PEML prepared using polyelectrolyte solutions containing each salt shown. Abbreviations for the salt anions are shown in Table S-5 and Chart 1, main text. Salt anions were typically present at 0.05 M levels in the deposition solutions, with the exception of MP (open diamond and circle), which was limited by gel formation to levels of ~0.011 M. Table S-5 lists the data plotted and additional information concerning the films.